AIMS Mathematics, 9(4): 9195–9210.
DOI: 10.3934/math.2024448
Received: 17 January 2024
Revised: 23 February 2024
Accepted: 28 February 2024
Published: 06 March 2024

http://www.aimspress.com/journal/Math

Research article

Managing heat transfer effectiveness in a Darcy medium with a vertically non-linear stretching surface through the flow of an electrically conductive non-Newtonian nanofluid

Mohammed Alrehili*

Department of Mechanical Engineering, Faculty of Engineering, University of Tabuk, Tabuk 71491, Saudi Arabia

* **Correspondence:** Email: malrehili@ut.edu.sa; Tel: +966506334725.

Abstract: This study encapsulated the research methodology utilized in the flow behaviors of Williamson nanofluid and analyzed the associated mass heat transfer. The study concentrated on examining the magnetohydrodynamic behavior of nanofluids in the presence of heat generation effects and the inclusion of dissipative energy on a vertical nonlinear stretching surface submerged within a Darcy porous medium. The rationale for including variable viscosity and variable conductivity in this research was to precisely evaluate the mechanisms of heat and mass transfer, particularly with regard to the fluctuations in fluid properties. The objective was to enhance the understanding of how these varying properties impact the overall heat and mass transfer processes. The initial formulation of the phenomenon, initially presented as partial differential equations, was transformed into ordinary differential equations by employing appropriate dimensionless variables. The ultimate streamlined version of the model was then numerically solved utilizing the shooting method. By employing the numerical shooting method, we portrayed nanofluid patterns in velocity, temperature, and concentration fields, alongside essential parameters such as skin friction coefficient, Sherwood number, and Nusselt number. The significant key findings highlighted that both the porous parameter and the magnetic number increasingly affected temperature and concentration distributions. Additionally, increasing the thermophoresis parameter resulted in higher concentration and corresponding temperature levels. Graphical presentation and physical explanations were used for analysis, and the study's outcomes were compared to existing literature, affirming a strong agreement that validated the solutions.

Keywords: Williamson nanofluid; heat mass transfer; porous medium; viscous dissipation; heat generation
Mathematics Subject Classification: 76S05, 76D50, 76A05, 65L10

1. Introduction

The analysis of heat transfer mechanism in a boundary layer flow owing to a continuous stretched surface has gained considerable attention due to its significance in various industrial applications such as plastic film production, glass fiber manufacturing, paper making, polymer sheet processing, and metal wire production. The examination of the fluid flow through a continuously stretched surface was first investigated by Sakiadis [1]. In many practical situations, it is not a requirement for the surface to be linear, as seen in the stretching of plastic sheets, for example. Consequently, a multitude of scholars [2–7] have delved into the various models of fluid flow generated by a nonlinear stretching surface.

Fluid flow within porous materials is widely applied across various domains, serving important functions in fields including fuel cell technology, filtration procedures, material manufacturing, oil detection, thermal energy management, and flow bed chromatography, among others. The simultaneous consideration of temperature distribution and heat transfer within the boundary layer of both Newtonian and non-Newtonian models in porous media, under diverse physical conditions, is recognized as a promising approach to enhance thermal efficiency. This approach is seen as an effective method for improving heat transfer performance. Numerous researchers have been actively engaged in studying fluid dynamics within porous media, spanning from Darcy porous media [8–12] to non-Darcy porous media [13, 14], tackling a range of unique challenges and scenarios.

Nanofluids are created by the suspension of nanoparticles, which are extremely small in size and are in conventional fluids such as ethylene glycol, water, and various types of oils. It is commonly recognized that the presence of nanoparticles alters the transport characteristics and enhances the heat transfer efficiency of nanofluids. The primary objective behind the advancement of nanofluids is to achieve the highest possible thermal conductivity with a minimal concentration of nanoparticles, accomplished by ensuring the uniform dispersion and stable suspension of these nanoparticles within the base fluids. In a groundbreaking contribution, Choi and Eastman [15] introduced the concept of nanofluid to characterize this novel class of heat transfer fluids rooted in nanotechnology. These nanofluids stand out for their enhanced thermal conductive properties compared to typical fluids. Buongiorno [16] formulated an analytical model that considers convective phenomenon within nanofluids while accounting for the influence of thermophoresis and the Brownian motion effect. With the aid of this model, it becomes feasible to conduct a theoretical examination of the fluid's effective heat transfer capabilities. A thorough explanation of the importance of nanofluid applications in various sectors and their crucial function can be obtained from the studies described in [17–19]. These investigations explore the broad application of nanofluids and offer comprehensive perspectives on their significance in several domains. Due to the inception of this novel idea, numerous scholars have examined the topic of nanofluids in different geometrical configurations, as documented in [20–26].

In previous researches, extensive investigations have been conducted on the behavior of non-Newtonian Williamson fluids and nanofluids separately, utilizing a variety of geometric configurations and considering various fluid properties. These studies have been carried out due to the significant implications of these fluids in diverse scientific domains. Overlooking the non-Newtonian Williamson nanofluid in the presence of heat generation near an impermeable, nonlinear vertical stretching sheet, while considering variable fluid properties; represents a notable research gap, as indicated by prior studies. Hence, the main aim and novelty of the present study is to reveal the unique attributes of flow

involving non-Newtonian Williamson nanofluids. This flow takes place over a vertically stretching sheet with nonlinear properties, and it is additionally complicated by the existence of a porous medium. Within the scope of this ongoing research endeavor, we have integrated several critical factors to assess their impact on the fluid's behavior. These factors encompass the phenomenon of viscous dissipation, the influence of an external magnetic field, variable fluid properties, and the effects of heat generation. We aim to comprehensively examine how these elements collectively shape the fluid's characteristics and behavior. An exhaustive examination of previously published papers reveals that no prior attempts have been made to explore the subject matter under investigation. However, it is worth noting that the diverse perspectives and phenomena elucidated in the current research are anticipated to yield highly dynamic interactions that transcend traditional disciplinary boundaries. These are the key, impactful questions that our current study can address.

i. How does the rheological behavior of the non-Newtonian Williamson nanofluid influence its flow characteristics within the context of a vertical stretching sheet?

ii. What are the key factors influencing the rates of heat and mass transfer within the present system?

iii. How does the presence of nanoparticles alter the boundary layer characteristics near the stretching sheet?

iv. What is the numerical approach capable of addressing the highly nonlinear nature of the system of equations governing the described problem?

v. What insights does this study offer toward comprehending the dynamics of heat and mass transfer phenomena within applications involving porous media?

2. Mathematical model of the flow regime

In this section, we aim to investigate how certain critical phenomena, such as viscous dissipation and heat generation, influence the steady, noncompressible, viscous flow of a two-dimensional Williamson nanofluid within the region where y is greater than zero. The present framework belongs to the category of the Buongiorno nanofluid model, which offers flexibility by not imposing restrictions on the choice of nanoparticles. Within this model, there is freedom in selecting the type of nanoparticles to be utilized. We opted for the Williamson Nanofluid model because it is well-suited to depict the intricate rheological characteristics of the complex fluids investigated in this study. This model adeptly handles phenomena such as shear-thinning and variations in viscosity, which are common attributes of non-Newtonian fluids, thereby rendering it ideal for our analytical purposes. This fluid motion occurs as it traverses a surface that undergoes nonlinear stretching, resulting in a variable velocity distribution expressed as $u_w = cx^{\alpha}$, where c is a constant and α is the exponent of stretching.

Select a Cartesian coordinate system in which the y-axis is positioned perpendicular to the sheet, and the x-axis runs approximately parallel to the vertical sheet, as illustrated in Figure 1.

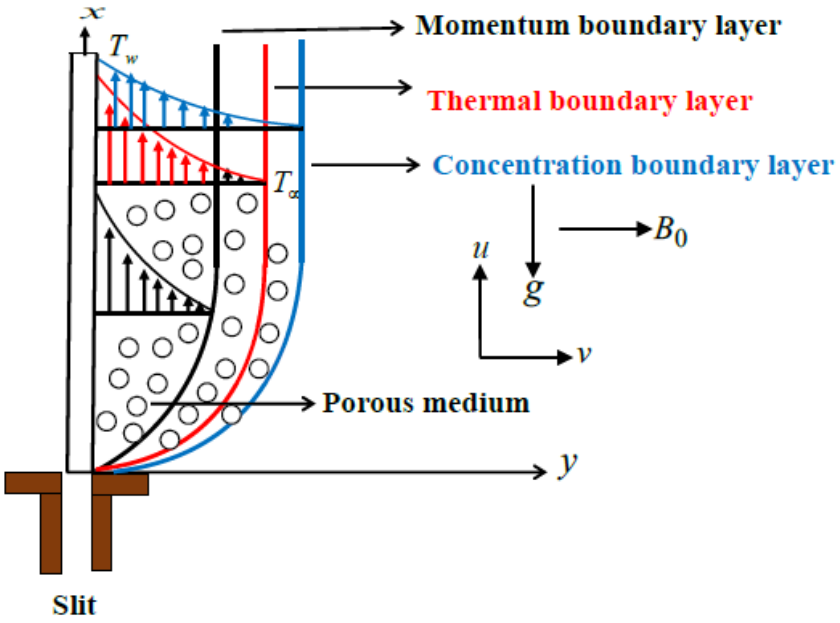

Figure 1. Flow configuration of the physical model.

Furthermore, we take into account the temperature distribution at the wall $T_w = T_\infty + C_1 x^r$ as well as the concentration distribution at the wall $C_w = C_\infty + C_2 x^s$, with C_1, C_2, r, s being positive constants, C_∞ is the nanofluid concentration away from the sheet, and T_∞ represents the temperature of the free stream fluid. During the motion of the nanofluid, a lateral magnetic field is present, characterized by the magnetic field strength $B = B_0 x^{\frac{\alpha-1}{2}}$. It's worth noting that any induced magnetic field is disregarded. We are accounting for the impact of changing viscosity and fluid conductivity in our analysis. Based on the references cited [27, 28], the governing equations are provided as follows:

$$\frac{\partial u}{\partial x} + \frac{\partial v}{\partial y} = 0, \tag{2.1}$$

$$u\frac{\partial u}{\partial x} + v\frac{\partial u}{\partial y} = g\beta_T(T - T_\infty) - \frac{\mu}{\rho_\infty k}u - \frac{\sigma B_0^2}{\rho_\infty}u + \frac{1}{\rho_\infty}\frac{\partial}{\partial y}\left(\mu\left[\frac{\partial u}{\partial y} + \frac{\Gamma}{\sqrt{2}}\left(\frac{\partial u}{\partial y}\right)^2\right]\right) + g\beta_C(C - C_\infty), \tag{2.2}$$

$$u\frac{\partial T}{\partial x} + v\frac{\partial T}{\partial y} = \frac{\mu}{\rho_\infty c_p}\left(\left(\frac{\partial u}{\partial y}\right)^2 + \frac{\Gamma}{\sqrt{2}}\left(\frac{\partial u}{\partial y}\right)^3\right) + \tau\left(D_B\frac{\partial C}{\partial y}\frac{\partial T}{\partial y} + \frac{D_T}{T_\infty}\left(\frac{\partial T}{\partial y}\right)^2\right) + \frac{Q}{\rho_\infty c_p}(T - T_\infty) + \frac{1}{\rho_\infty c_p}\frac{\partial}{\partial y}\left(\kappa\frac{\partial T}{\partial y}\right), \tag{2.3}$$

$$u\frac{\partial C}{\partial x} + v\frac{\partial C}{\partial y} = \frac{D_T}{T_\infty}\frac{\partial^2 T}{\partial y^2} + D_B\frac{\partial^2 C}{\partial y^2}. \tag{2.4}$$

It's important to note that the pressure term is particularly noticeable in Eq (2.2), specifically within the segments relating to the ambient temperature T_∞ and concentration C_∞. The variables u and v correspond to the velocity components along the x and y axes, respectively. ρ_∞ denotes the ambient density of the Williamson nanofluid, K represents the permeability of the porous medium, and T

signifies the temperature of the Williamson fluid. The variable C denotes the concentration of the nanofluid, c_p is the specific heat at constant pressure, and the symbol τ represents the fraction of the heat capacity of the nanomaterial relative to that of the surrounding fluid. D_T stands for the diffusion coefficient related to thermophoresis, which quantifies the motion of particles in response to temperature gradients. Q represents the volumetric heat generation in dimensional terms, indicating the amount of heat produced per unit volume. D_B signifies the coefficient associated with Brownian motion, which characterizes the random movement of particles suspended in a fluid due to thermal fluctuations. The conditions of the Williamson nanofluid flow are as follows:

$$v = 0, \quad u = cx^{\alpha}, \quad T_w = C_1 x^r + T_\infty, \quad C_w = C_2 x^s + C_\infty \quad at \quad y = 0, \tag{2.5}$$

$$u \to 0, \quad T \to T_\infty, \quad C \to C_\infty, \quad as \quad y \to \infty. \tag{2.6}$$

Our study's Eqs (2.5) and (2.6) represent specific physical assumptions. Equation 5's ($v = 0$) term indicates impermeability of the sheet, resulting in no suction velocity. Furthermore, the mathematical forms of T_w and C_w suggest they vary with x. Equation (2.6) describes constants for velocity $u \to 0$, temperature $T \to T_\infty$, and concentration $C \to C_\infty$ away from the sheet. Equations (2.2) through (2.4) are converted into ordinary differential equations by using the specified transformation variables [28]:

$$\psi(x, y) = \sqrt{\frac{cx^{\alpha+1}\mu_\infty}{\rho_\infty}} f(\eta), \quad \eta = \sqrt{\frac{c\rho_\infty x^{\alpha-1}}{\mu_\infty}} y, \tag{2.7}$$

$$\phi(\eta) = \frac{C - C_\infty}{C_w - C_\infty}, \quad \theta(\eta) = \frac{T - T_\infty}{T_w - T_\infty}. \tag{2.8}$$

Here, the variable η serves as the dimensionless similarity variable, $f(\eta)$ describes the dimensionless stream function, $\phi(\eta)$ represents the dimensionless concentration, and $\theta(\eta)$ symbolizes the dimensionless temperature. Moreover, in this study, we propose that the thermal conductivity κ and viscosity μ of the Williamson nanofluid depend on the dimensionless temperature, and this relationship is expressed by the following equation [29]:

$$\mu = \mu_\infty e^{-n\theta}, \quad \kappa = \kappa_\infty(1 + \lambda\theta). \tag{2.9}$$

As previously discussed in the literature [29], representing fluid viscosity exponentially with respect to temperature is employed to address the substantial variations in viscosity observed with minor temperature fluctuations. Here, we use λ to represent the thermal conductivity parameter, and n is employed as the viscosity parameter. κ_∞ is indicative of the constant thermal conductivity of the Williamson nanofluid at standard ambient conditions, while μ_∞ denotes the unchanging viscosity of the Williamson nanofluid under the same ambient conditions. After implementing the transformations as described in Eq (2.7), it becomes evident that the continuity equation presented in Eq (2.1) is easily and promptly fulfilled. Additionally, by applying the identical nondimensional transformations discussed previously in (2.7) and (2.8), we can establish the following equations:

$$\begin{aligned}\left(f'''(1 + \Gamma_w f'') - n\left(1 + \frac{\Gamma_w}{2} f''\right)\theta' f''\right)e^{-n\theta} - \alpha f'^2 + \left(\frac{\alpha+1}{2}\right) ff'' + \delta_T\theta + \delta_C\phi \\ - P_k e^{-n\theta} f' - Mf' = 0,\end{aligned} \tag{2.10}$$

$$\frac{1}{Pr}\left(\theta''(1+\lambda\theta)+\lambda\theta'^2\right)-rf'\theta+\left(\frac{\alpha+1}{2}\right)f\theta'+W_b\,\theta'\phi'+W_t\,\theta'^2+\gamma\,\theta + Ec\,e^{-n\theta}\left(1+\frac{\Gamma_w}{2}f''\right)f''^2=0, \tag{2.11}$$

$$\phi''+\frac{W_t}{W_b}\theta''+Sc\left[\left(\frac{\alpha+1}{2}\right)f\phi'-s\,f'\phi\right]=0. \tag{2.12}$$

Likewise, the boundary conditions under consideration are:

$$f=0,\qquad \theta=\phi=f'=1,\qquad at\quad \eta=0, \tag{2.13}$$

$$\theta\to 0,\qquad f'\to 0,\qquad \phi\to 0,\qquad \text{at}\qquad \eta\to\infty. \tag{2.14}$$

The parameters mentioned in Eqs (2.10) to (2.12) are explicitly described and defined as the local Williamson fluid parameter Γ_e, the porous parameter P_k, the mixed convection parameter δ_T, the modified mixed convection parameter δ_C, the Eckert number Ec, the Prandtl number Pr, the heat generation parameter γ, the thermophoresis parameter W_t, the magnetic parameter M, the Schmidt number Sc, and the Brownian motion parameter W_b. Moreover, these controlling factors are delineated as follows:

$$\Gamma_e=\left(\frac{\sqrt{2}x^{\frac{3\alpha-1}{2}}c^{\frac{3}{2}}}{\sqrt{\nu_\infty}}\right)\Gamma,\quad P_k=\frac{\mu_\infty u_w^2}{c^3\,k\,\rho_\infty},\quad \delta_T=\frac{g\beta_T C_1\nu_\infty Re_x}{c^2u_w},\quad \delta_C=\frac{g\beta_C C_2\nu_\infty Re_x}{c^2u_w}, \tag{2.15}$$

$$Ec=\frac{u_w^2}{c_p(T_w-T_\infty)},\quad Pr=\frac{\mu_\infty c_p}{\kappa_\infty},\quad \gamma=\frac{Q}{u_w\rho_\infty c_p},\quad W_t=\frac{\tau\rho_\infty D_T\,(T_w-T_\infty)}{\mu_\infty T_\infty}, \tag{2.16}$$

$$M=\frac{\sigma B_0^2}{c\rho_\infty},\quad Sc=\frac{\mu_\infty}{\rho_\infty D_B},\quad W_b=\frac{\tau\rho_\infty D_B\,(C_w-C_\infty)}{\mu_\infty}. \tag{2.17}$$

It's crucial to remember in this regard that the parameter values selected for this investigation take into consideration the physical characteristics of the nanofluid, boundary conditions, and outcomes of earlier studies. Furthermore, a few values match theoretical predictions. The key quantities of interest in this investigation include the skin friction coefficient Cf_x, the local Nusselt number Nu_x, and the local Sherwood number Sh_x. These parameters are defined as follows:

$$Cf_x=-2Re_x^{\frac{-1}{2}}\left(1+\frac{\Gamma_e}{2}f''(0)\right)f''(0)e^{-n},\quad Nu_x=-Re_x^{\frac{1}{2}}\theta'(0),\quad Sh_x=-Re_x^{\frac{1}{2}}\phi'(0), \tag{2.18}$$

where $Re_x=\frac{u_w\rho_\infty x}{\mu_\infty}$ is the local Reynolds number.

3. Potential sources of error

When evaluating the numerical solution using the shooting method, it's crucial to recognize potential sources of error or uncertainty that might impact result accuracy. Numerous factors could contribute to these inaccuracies:

i. Boundary Conditions: Inaccurate boundary conditions can greatly affect solution accuracy; they are pivotal in defining the problem domain and require careful consideration.

ii. Convergence Criteria: Wrong convergence criteria in iterative methods can cause early termination or excessive iterations, resulting in inaccurate solutions.

iii. Numerical Round-off Errors: Limited precision in numerical computations can lead to error accumulation, especially in lengthy simulations or when dealing with extremely small or large values.

iv. Model Validation: Absence of validation against theoretical data or benchmark solutions can erode trust in the numerical outcomes.

4. Verification of the physical model

Table 1 provides a comparative analysis between the findings of our present study and the results previously reported in the literature. This comparative assessment is conducted to validate the accuracy and reliability of our numerical solution. It's worth mentioning that a strong concordance is observed between the results obtained in our present study and those previously established in the literature. As a consequence of this robust alignment between the outcomes, the validation of our current results is effectively guaranteed.

Table 1. Values of Nusselt number $-\theta'(0)$ for various values of Pr when $\Gamma_e = \delta_T = \delta_C = r = P_k = M = W_t = W_b = Ec = 0$ and $\lambda = 0, \alpha = 1.0$.

Pr	Abbas et al. ([28])	Present work
0.07	0.065542	0.065541887990
0.20	0.169128	0.169127632145
2.00	0.911368	0.911367598850

5. Graphical and tabulated results accompanied by explanations

The present section elucidates the underlying physical phenomena that transpired within the flow regime during computations of the velocity field $f'(\eta)$, temperature distribution $\theta(\eta)$, and mass concentration $\phi(\eta)$. This analysis encompasses a wide range of values for flow parameters that serve to define and characterize the flow characteristics. In addition, we have computed and organized the values for the skin friction coefficient $\frac{Cf_x}{2}Re_x^{\frac{1}{2}}$, Nusselt number $\frac{Nu_x}{\sqrt{Re_x}}$, and Sherwood number $\frac{Sh_x}{\sqrt{Re_x}}$ in tabular format. We have graphically presented all the obtained results, mapping them across various flow parameters, including the porous medium parameter P_k, the magnetic number M, Williamson parameter Γ_w, thermophoresis parameter W_t, mixed convection parameter δ_T, modified convection parameter δ_C, heat generation parameter γ, Eckert number Ec, and the Brownian motion parameter W_b. This graphical representation provides a comprehensive visualization of how the results vary with respect to these key flow parameters. Figure 2 has been constructed to illustrate the variations in the velocity field, temperature field, and mass concentration. These variations are depicted with respect to a wide range of values for the porous parameter P_k, while keeping the values of other parameters fixed and constant. The observation reveals that as the value of the porous parameter increases, it causes a

creation in the decreasing pattern in nanofluid velocity. Instead, it instigates an upward trajectory in temperature and concentration.

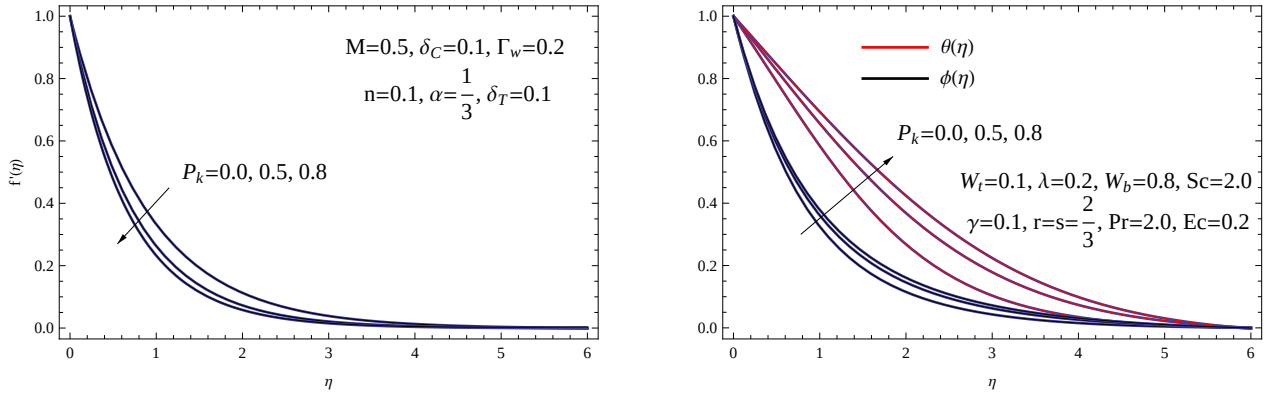

Figure 2. (a) $f'(\eta)$ for various P_k; (b) $\phi(\eta)$ and $\theta(\eta)$ for various P_k.

Figure 3 illustrates the influence of the magnetic number, denoted as M, on the functions $f'(\eta)$, $\theta(\eta)$, and $\phi(\eta)$. It visually represents how changes in the magnetic number affect these functions. The graphical representation provides a visual insight into the fact that an increase in the magnetic number, denoted as M, leads to a reduction in the function $f'(\eta)$. Conversely, there is a contrasting trend for both concentration $\phi(\eta)$ and temperature $\theta(\eta)$. These behaviors are a consequence of the generation of the Lorentz force, which opposes the flow of the nanofluid and subsequently influences these variables in the described manner. Further, Ali et al. [30–34] thoroughly explored the characteristics of the Lorentz force generated within a magnetic field. Their study focused on elucidating the influence of this force on the rates of heat and mass transfer. Their work offered a comprehensive examination of the interaction between magnetic fields and the Lorentz force, offering detailed insights into how it affects the transfer mechanisms.

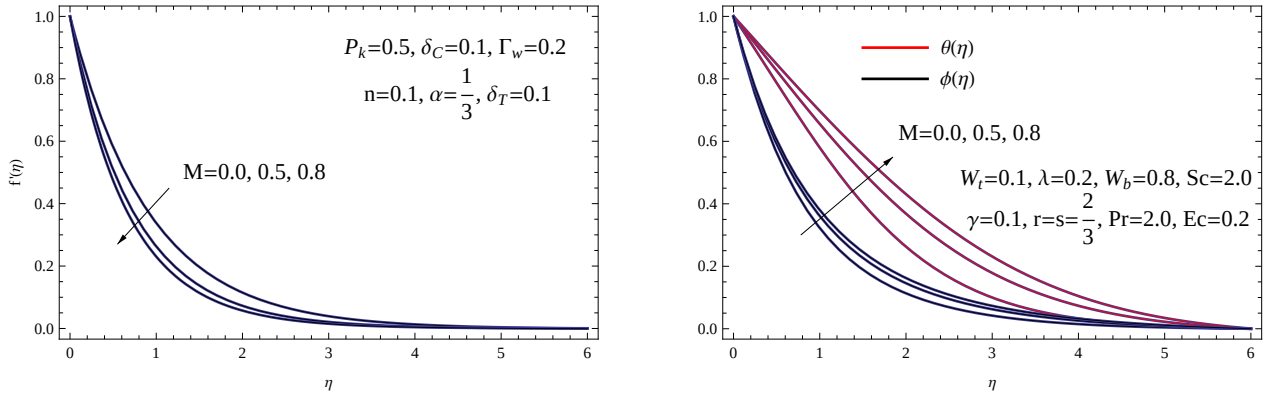

Figure 3. (a) $f'(\eta)$ for various M; (b) $\phi(\eta)$ and $\theta(\eta)$ for various M.

Figure 4 depicts the influence of the Williamson nanofluid parameter, denoted as Γ_w, on the profiles of velocity $f'(\eta)$, temperature $\theta(\eta)$, and concentration $\phi(\eta)$. These figures provide a visual representation of how changes in the Williamson parameter affect the behavior of these profiles. As observed in the graphical representations, augmenting the Williamson nanofluid parameter has a dual effect. It causes a decrease in the velocity of the nanofluid while simultaneously resulting in an increase in both concentration and temperature. Physically, an increase in Γ_w results in lower fluid viscosity,

enabling freer nanoparticle movement. This increased mobility substantially boosts the nanoparticle concentration in the fluid.

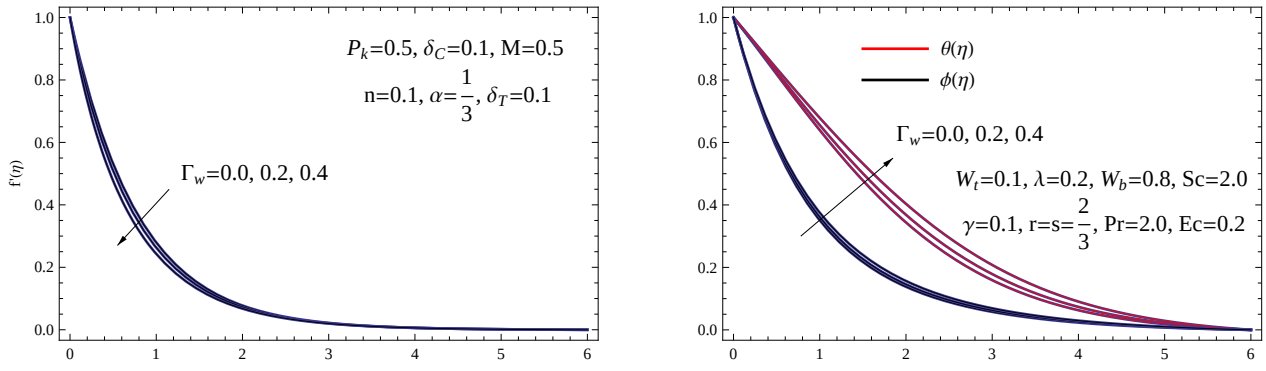

Figure 4. (a) $f'(\eta)$ for various Γ_w; (b) $\phi(\eta)$ and $\theta(\eta)$ for various Γ_w.

Figure 5 is presented to visually represent the relationships between the velocity field $f'(\eta)$, temperature field $\theta(\eta)$, and mass concentration $\phi(\eta)$ as functions of various values of the mixed convection parameter δ_T. These illustrations are generated while keeping the values of other parameters constant. The graphs offer a clear visual depiction of the relationship between an augmented mixed convection parameter and the following outcomes: An increase in the function $f'(\eta)$ and a simultaneous decrease in both $\phi(\eta)$ and $\theta(\eta)$. These trends are clearly illustrated in the graphical representations. Physically, greater mixed convection parameter causes the buoyancy-driven and forced convection to interact more strongly, thereby boosting the velocity of the nanofluid. The fluid movements and velocities in the nanofluid enhance as this parameter rises, owing to the strengthening of both forced and natural convection.

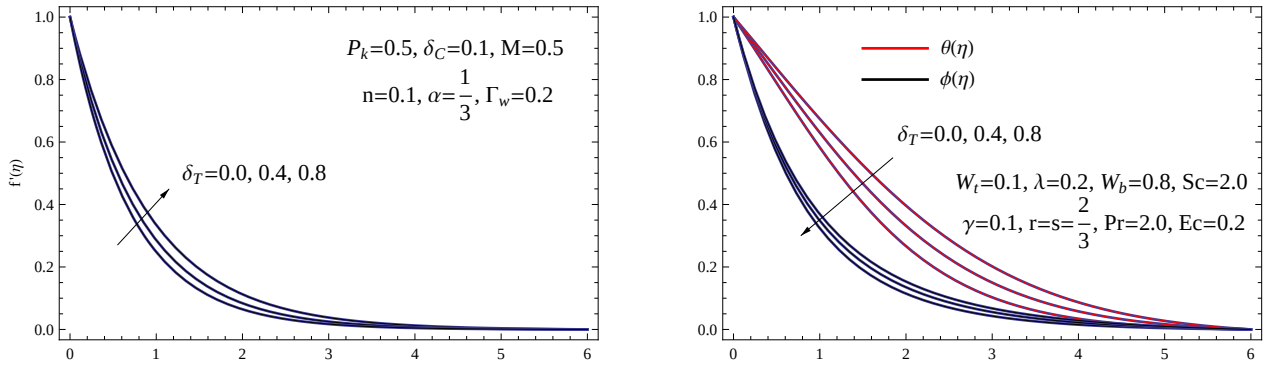

Figure 5. (a) $f'(\eta)$ for various δ_T; (b) $\phi(\eta)$ and $\theta(\eta)$ for various δ_T.

Figure 6 is sketched for $f'(\eta)$, $\theta(\eta)$, and $\phi(\eta)$, respectively, against different values of the modified mixed convection parameter δ_C. The momentum boundary layer thickness is thickened, whereas the thermal boundary layer is thinner and accompanied with enhancement in the velocity field and a decrease in both concentration and temperature fields, with increasing in the modified mixed convection parameter δ_C. Physically, better fluid motion and mixing cause the nanofluid concentration to drop with a boosting modified mixed convection factor. Fluid motion is enhanced as this parameter rises because of a stronger interplay between forced convection and buoyancy-driven flow. Reduced total concentrations are the outcome of the more uniform dispersion of nanoparticles in the fluid caused by this higher velocity.

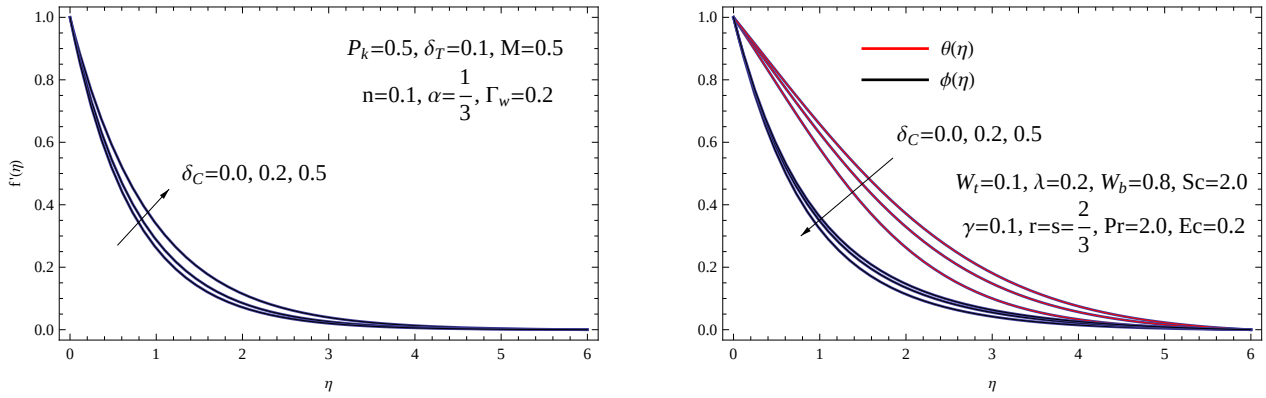

Figure 6. (a) $f'(\eta)$ for various δ_C; (b) $\phi(\eta)$ and $\theta(\eta)$ for various δ_C.

The impact of the heat generation parameter γ on the temperature distribution $\theta(\eta)$ is illustrated in detail in Figure 7(a). It has been observed that when the heat generation parameter γ is augmented, there is a discernible increase in the temperature distribution $\theta(\eta)$, and this increase is of a significant magnitude. The physical response of the temperature distribution $\theta(\eta)$ concerning the parameter Ec is depicted in Figure 7(b). The elevation of the Ec parameter results in an ascending trend in the behavior of the thermal thickness and the temperature distribution $\theta(\eta)$. Physically, viscous dissipation transforms heat energy into mechanical energy. When Ec is raised, more forces work to dissipate viscosity, causing the fluid to expend additional energy, thus raising its temperature.

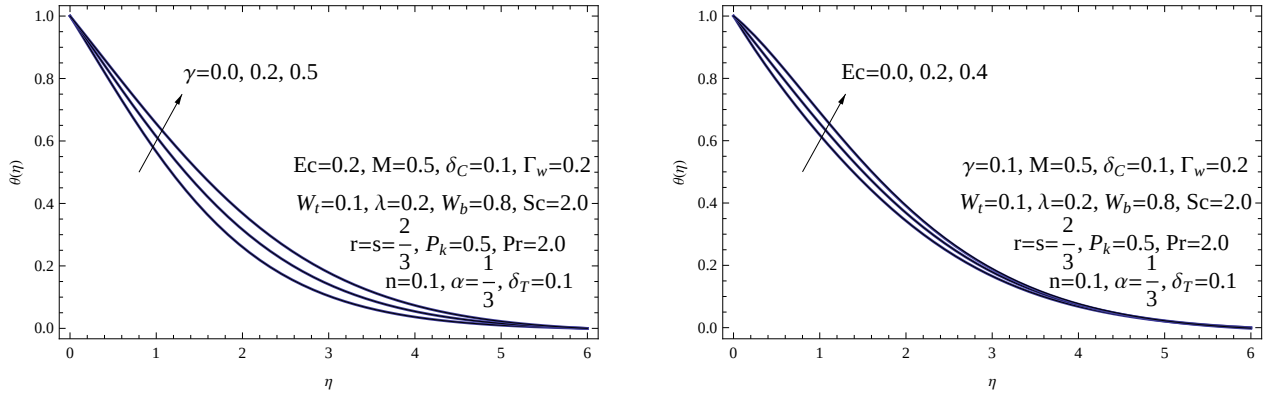

Figure 7. (a) $\theta(\eta)$ for various γ; (b) $\theta(\eta)$ for various Ec.

Figure 8 provides a visual depiction of the impact of the Brownian motion parameter W_b on the characteristics of velocity, concentration, and temperature within a given context. The illustrated sketches make it clear that when we increase the value of the Brownian motion parameter, denoted as W_b, there is a swift and substantial intensification in the temperature field. In contrast, a contrasting pattern is observed for the concentration field, where an opposite trend is evident as the parameter W_b increases. In physical terms, the primary factor influencing the Brownian motion parameter is the difference in nanofluid concentration between the surface and the surrounding area. Therefore, when the Brownian motion parameter is raised, these concentration variations become more pronounced, leading to a decrease in the concentration field within the nanofluid flow.

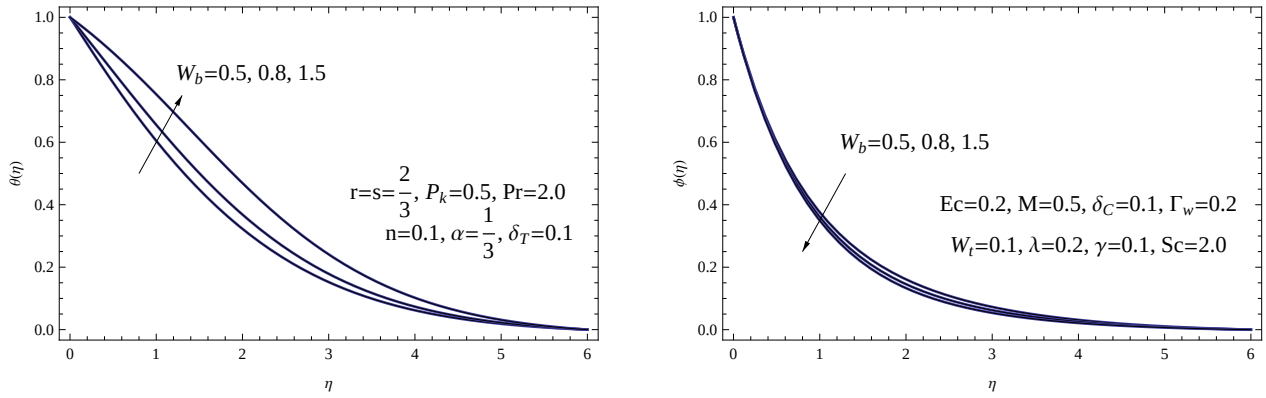

Figure 8. (a) $\theta(\eta)$ for various W_b; (b) $\phi(\eta)$ for various W_b.

Figure 9 illustrates the influence of the thermophoresis parameter W_t on the functions $\theta(\eta)$ and $\phi(\eta)$. It shows how changes in the thermophoresis parameter affect the behavior of these functions. We can observe that an increase in the thermophoresis parameter leads to an augmentation in both $\phi(\eta)$ and $\theta(\eta)$. In physical terms, the disparity in fluid temperature near the sheet compared to its surroundings induces a heating effect on the nanofluid. This heating effect, in turn, leads to an escalation in both the fluid temperature and the convective transport phenomenon as W_t increases.

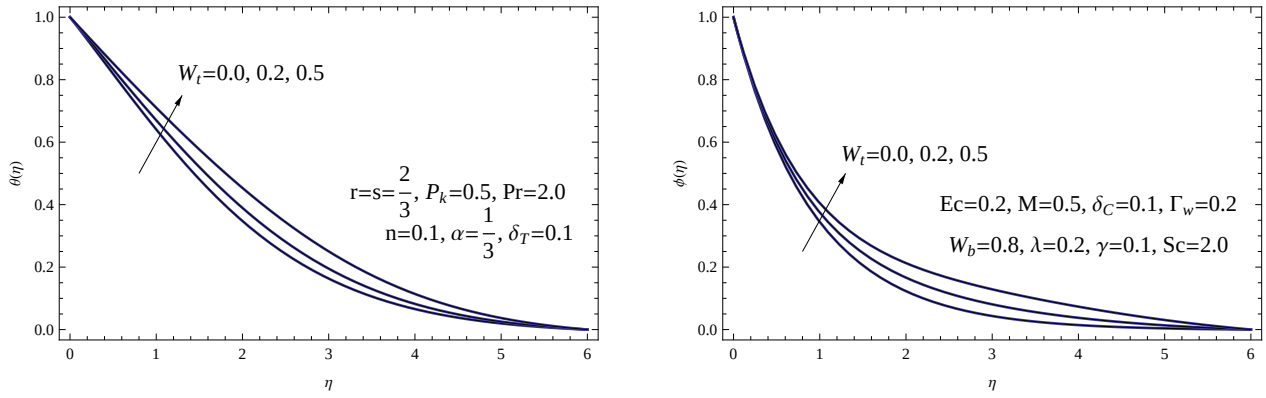

Figure 9. (a) $\theta(\eta)$ for various W_t; (b) $\phi(\eta)$ for various W_t.

Table 2 provides a visual representation of how the controlling parameters influence the values of the skin friction coefficient $\frac{Cf_x}{2}Re_x^{\frac{1}{2}}$, the Nusselt number $\frac{Nu_x}{\sqrt{Re_x}}$, and the Sherwood number $\frac{Sh_x}{\sqrt{Re_x}}$. It shows the impact of these parameters on these relevant quantities. The findings suggest that as both the magnetic and porous parameters are elevated, there is an increase in the skin friction coefficient. However, this rise in these parameters results in an attenuation in both the Nusselt number and the Sherwood number. Similarly, the table reveals that when the Williamson parameter is raised, it results in a reduction in the values of $\frac{Cf_x}{2}Re_x^{\frac{1}{2}}$, $\frac{Nu_x}{\sqrt{Re_x}}$, and $\frac{Sh_x}{\sqrt{Re_x}}$. When you raise the values of either the mixed convection parameter or the modified mixed convection parameter, the shear stress also increases. However, both the local Nusselt number and the local Sherwood number decrease when these parameters are increased. The local skin friction coefficient and the local Nusselt number both decrease as the Brownian motion parameter increases. In contrast, the local Sherwood number shows the opposite trend with the same parameter.

Table 2. Values of $\frac{Cf_x}{2}Re_x^{\frac{1}{2}}$, $\frac{Sh_x}{\sqrt{Re_x}}$, and $\frac{Nu_x}{\sqrt{Re_x}}$ for the controlling parameters with $Pr = 2.0$ and $Sc = 2.0$.

P_k	M	Γ_w	δ_T	δ_C	γ	Ec	W_b	W_t	$\frac{Cf_x}{2}Re_x^{\frac{1}{2}}$	$\frac{Nu_x}{\sqrt{Re_x}}$	$\frac{Sh_x}{\sqrt{Re_x}}$
0.0	0.5	0.2	0.1	0.1	0.1	0.2	0.8	0.1	0.888287	0.410011	1.15017
0.5	0.5	0.2	0.1	0.1	0.1	0.2	0.8	0.1	1.071350	0.338644	1.08916
0.8	0.5	0.2	0.1	0.1	0.1	0.2	0.8	0.1	1.164841	0.299165	1.05899
0.5	0.0	0.2	0.1	0.1	0.1	0.2	0.8	0.1	0.871137	0.414891	1.15461
0.5	0.5	0.2	0.1	0.1	0.1	0.2	0.8	0.1	1.071350	0.338644	1.08916
0.5	0.8	0.2	0.1	0.1	0.1	0.2	0.8	0.1	1.173052	0.295217	1.05646
0.5	0.5	0.0	0.1	0.1	0.1	0.2	0.8	0.1	1.125861	0.351083	1.10911
0.5	0.5	0.2	0.1	0.1	0.1	0.2	0.8	0.1	1.071350	0.338644	1.08916
0.5	0.5	0.4	0.1	0.1	0.1	0.2	0.8	0.1	0.999922	0.319165	1.06004
0.5	0.5	0.2	0.0	0.1	0.1	0.2	0.8	0.1	0.877252	0.412269	1.15214
0.5	0.5	0.2	0.4	0.1	0.1	0.2	0.8	0.1	1.002551	0.365263	1.11076
0.5	0.5	0.2	0.8	0.1	0.1	0.2	0.8	0.1	1.112012	0.320275	1.07494
0.5	0.5	0.2	0.1	0.0	0.1	0.2	0.8	0.1	0.871137	0.414891	1.15461
0.5	0.5	0.2	0.1	0.2	0.1	0.2	0.8	0.1	1.000963	0.376618	1.10192
0.5	0.5	0.2	0.1	0.5	0.1	0.2	0.8	0.1	1.075452	0.336646	1.08758
0.5	0.5	0.2	0.1	0.1	0.0	0.2	0.8	0.1	1.074250	0.443443	1.08027
0.5	0.5	0.2	0.1	0.1	0.2	0.2	0.8	0.1	1.072672	0.384186	1.08532
0.5	0.5	0.2	0.1	0.1	0.5	0.2	0.8	0.1	1.071355	0.338643	1.08916
0.5	0.5	0.2	0.1	0.1	0.1	0.0	0.8	0.1	1.073052	0.458483	1.07705
0.5	0.5	0.2	0.1	0.1	0.1	0.2	0.8	0.1	1.071350	0.338644	1.08916
0.5	0.5	0.2	0.1	0.1	0.1	0.4	0.8	0.1	1.069693	0.219425	1.10134
0.5	0.5	0.2	0.1	0.1	0.1	0.2	0.5	0.1	1.073161	0.431002	1.06592
0.5	0.5	0.2	0.1	0.1	0.1	0.2	0.8	0.1	1.071350	0.338644	1.08916
0.5	0.5	0.2	0.1	0.1	0.1	0.2	1.5	0.1	1.068091	0.202057	1.10345
0.5	0.5	0.2	0.1	0.1	0.1	0.2	0.8	0.0	1.071901	0.351958	1.10531
0.5	0.5	0.2	0.1	0.1	0.1	0.2	0.8	0.2	1.070832	0.326233	1.07476
0.5	0.5	0.2	0.1	0.1	0.1	0.2	0.8	0.5	1.069421	0.293593	1.04058

6. Conclusions

The present research focuses on the analysis of the flow and heat-mass transfer characteristics of a non-Newtonian Williamson nanofluid. This nanofluid is subjected to a nonlinear vertical stretching sheet, which is positioned within a Darcy porous medium. The study also takes into account the effects of magnetic field, viscous dissipation, and heat generation on the system. Additionally, certain properties of the nanofluid, such as viscosity and conductivity, are hypothesized to change in response to temperature variations. The equation, once transformed into a set of ordinary differential equations, is tackled through the application of the shooting method. Subsequently, the findings are depicted

graphically to illustrate the results. The key findings derived from the presented results are succinctly summarized as follows:

(1) Both the magnetic number and the porous parameter exhibit a growing influence on the temperature and concentration distributions within the nanofluid.
(2) As the modified convection parameter, thermophoresis, and magnetic number are all increased, both the Nusselt and Sherwood numbers decrease.
(3) Augmenting the Williamson nanofluid parameter resulted in a decrease in both the skin friction coefficient and the velocity of the nanofluid flow.
(4) Augmenting the thermophoresis parameter leads to a rise in both the concentration and the corresponding temperature of the Williamson nanofluid.
(5) The Brownian motion parameter has contrasting effects on both the concentration and temperature of the nanofluid.
(6) Future directions in this field of study could include hybrid Williamson nanofluids under variable density and Ohmic heating, which could be a major area of interest.

Use of AI tools declaration

The author declares that he has not used Artificial Intelligence (AI) tools in the creation of this article.

Acknowledgments

The author sincerely thanks the Faculty of Engineering, University of Tabuk for their continuous support of scientific research and valuable contributions.

Additionally, gratitude is extended to the editor and referees for their insightful comments and suggestions, which have greatly improved the paper's quality.

Conflict of interest

The author declares no conflicts of interest.

References

1. B. C. Sakiadis, Boundary layer behavior on continuous solid flat surfaces, *Am. Inst. Chem. Eng. J.*, **7** (1961), 26–28. https://doi.org/10.1002/aic.690070108
2. R. Cortell, Viscous flow and heat transfer over a nonlinearly stretching sheet, *Appl. Math. Comput.*, **184** (2007), 864–873. https://doi.org/10.1016/j.amc.2006.06.077
3. A. M. Megahed, Variable viscosity and slip velocity effects on the flow and heat transfer of a power-law fluid over a non-linearly stretching surface with heat flux and thermal radiation, *Rheol. Acta*, **51** (2012), 841–874. https://doi.org/10.1007/s00397-012-0644-8
4. P. K. Kameswaran, P. Sibanda, M. K. Partha, P. Murthy, Thermophoretic and nonlinear convection in non-Darcy porous medium, *ASME J. Heat Mass Tran.*, **136** (2014), 042601. https://doi.org/10.1115/1.4025902

5. A. M. Megahed, Carreau fluid flow due to nonlinearly stretching sheet with thermal radiation, heat flux, and variable conductivity, *Appl. Math. Mechan.*, **40** (2019), 1615–1624. https://doi.org/10.1007/s10483-019-2534-6

6. G. Rasool, A. Shafiq, M. S. Alqarni, A. Wakif, I. Khan, M. S. Bhutta, Numerical scrutinization of Dar-cy-Forchheimer relation in convective magnetohydrodynamic nanofluid flow bounded by nonlinear stretching surface in the perspective of heat and mass transfer, *Micromachines*, **12** (2021), 374. https://doi.org/10.3390/mi12040374

7. S. M. Abo-Dahab, M. A. Abdelhafez, F. M. Oudina, S. M. Bilal, MHD Casson nanofluid flow over nonlinearly heated porous medium in presence of extending surface effect with suction/injection, *Indian J. Phys.*, **95** (2021), 2703–2717. https://doi.org/10.1007/s12648-020-01923-z

8. K. Vafai, C. L. Tien, Boundary and inertia effects on flow and heat transfer in porous media, *Int. J. Heat Mass Tran.*, **24** (1981), 195–203. https://doi.org/10.1016/0017-9310(81)90027-2

9. P. X. Jiang, Z. P. Ren, Numerical investigation of forced convection heat transfer in porous media using a thermal non-equilibrium model, *Int. J. Heat Fluid Fl.*, **22** (2001), 102–110. https://doi.org/10.1016/S0142-727X(00)00066-7

10. M. Kothandapani, S. Srinivas, On the influence of wall properties in the MHD peristaltic transport with heat transfer and porous medium, *Phys. Lett. A*, **372** (2008), 4586–4591. https://doi.org/10.1016/j.physleta.2008.04.050

11. R. A. Mahdi, H. A. Mohammed, K. M. Munisamy, N. H. Saeid, Review of convection heat transfer and fluid flow in porous media with nanofluid, *Renew. Sust. Energ. Rev.*, **41** (2015), 715–734. https://doi.org/10.1016/j.rser.2014.08.040

12. W. Abbas, A. M. Megahed, Powell-Eyring fluid flow over a stratified sheet through porous medium with thermal radiation and viscous dissipation, *AIMS Math.*, **6** (2021), 13464–13479. https://doi.org/10.3934/math.2021780

13. K. Sharma, L. Kumar, A. Singh, V. K. Joshi, Mixed convection flow over non-Darcy porous stretching/shrinking sheet, *Indian J. Chem. Techn.*, **30** (2023), 746–752. https://doi.org/10.56042/ijct.v30i6.487

14. K. Sharma, L. Kumar, A. Singh, V. K. Joshi, Dynamics of MHD Casson fluid in non-Darcy porous medium: The impact of thermal radiation, Dufour-Soret, and chemical reaction, *Mod. Phys. Lett. B*, 2023. https://doi.org/10.1142/S0217984923410075

15. S. Choi, J. A. Eastman, Enhancing thermal conductivity of fluid with nanoparticles, developments and applications of non-Newtonian flow, *ASME FED*, **231** (1995), 99–105. https://www.osti.gov/biblio/196525

16. J. Buongiorno, Convective transport in nanofluids, *AMSE J. Heat Mass Tran.*, **128** (2006), 240–250. https://doi.org/10.1115/1.2150834

17. M. M. Bhatti, K. Vafai, S. I. Abdelsalam, The role of nanofluids in renewable energy engineering, *Nanomaterials*, **13** (2023), 2671. https://doi.org/10.3390/nano13192671

18. S. I. Abdelsalam, A. Z. Zaher, Biomimetic amelioration of zirconium nanoparticles on a rigid substrate over viscous slime - a physiological approach, *Appl. Math. Mech.*, **44** (2023), 1563–1576. https://doi.org/10.1007/s10483-023-3030-7

19. S. I. Abdelsalam, A. M. Alsharif, Y. A. Elmaboud, A. I. Abdellateef, Assorted kerosene-based nanofluid across a dual-zone vertical annulus with electroosmosis, *Heliyon*, **9** (2023), e15916. https://doi.org/10.1016/j.heliyon.2023.e15916

20. N. A. M. Noor, S. Shafie, M. A. Admon, Slip effects on MHD squeezing flow of Jeffrey nanofluid in horizontal channel with chemical reaction, *Mathematics*, **9** (2021), 1215. https://doi.org/10.3390/math9111215

21. N. S. Yousef, A. M. Megahed, N. I. Ghoneim, M. Elsafi, E. Fares, Chemical reaction impact on MHD dissipative Casson-Williamson nanofluid flow over a slippery stretching sheet through porous medium, *Alex. Eng. J.*, **61** (2022), 10161–10170. https://doi.org/10.1016/j.aej.2022.03.032

22. M. Alrehili, Development for cooling operations through a model of nanofluid flow with variable heat flux and thermal radiation, *Processes*, **10** (2023), 2650. https://doi.org/10.3390/pr10122650

23. S. Sadighi, H. Afshar, M. Jabbari, H. A. D. Ashtiani, Heat and mass transfer for MHD nanofluid flow on a porous stretching sheet with prescribed boundary conditions, *Case Stud. Therm. Eng.*, **49** (2023), 103345. https://doi.org/10.1016/j.csite.2023.103345

24. M. Alrehili, Slippery flow of non-Newtonian Maxwell thermal nanofluid past a permeable vertically stretched sheet through a porous medium, *Eur. Phys. J. Plus*, **138** (2023), 444. https://doi.org/10.1140/epjp/s13360-023-04050-w

25. M. Alrehili, Improvement for engineering applications through a dissipative Carreau nanofluid fluid flow due to a nonlinearly stretching sheet with thermal radiation, *Case Stud. Therm. Eng.*, **42** (2023), 102768. https://doi.org/10.1016/j.csite.2023.102768

26. N. Vijay, K. Sharma, Dynamics of stagnation point flow of Maxwell nanofluid with combined heat and mass transfer effects: A numerical investigation, *Int. Commun. Heat Mass*, **141** (2023), 106545. https://doi.org/10.1016/j.icheatmasstransfer.2022.10

27. A. M. Megahed, Williamson fluid flow due to a nonlinearly stretching sheet with viscous dissipation and thermal radiation, *J. Egypt. Math. Soc.*, **27** (2019), 12. https://doi.org/10.1186/s42787-019-0016-y

28. A. Abbas, M. B. Jeelani, A. S. Alnahdi, A. Ilyas, MHD Williamson nanofluid fluid flow and heat transfer past a non-linear stretching sheet implanted in a porous medium: Effects of heat generation and viscous dissipation, *Processes*, **10** (2022), 1221. https://doi.org/10.3390/pr10061221

29. A. M. Megahed, Improvement of heat transfer mechanism through a Maxwell fluid flow over a stretching sheet embedded in a porous medium and convectively heated, *Math. Comput. Simulat.*, **187** (2021), 97–109. https://doi.org/10.1016/j.matcom.2021.02.018

30. B. Ali, I. Siddique, I. Khan, B. Masood, S. Hussain, Magnetic dipole and thermal radiation effects on hybrid base micropolar CNTs flow over a stretching sheet: Finite element method approach, *Results Phys.*, **25** (2021), 104145. https://doi.org/10.1016/j.rinp.2021.104145

31. B. Ali, A. Shafiq, I. Siddique, Q. Al-Mdallal, F. Jarad, Significance of suction/injection, gravity modulation, thermal radiation, and magnetohydrodynamic on dynamics of micropolar fluid subject to an inclined sheet via finite element approach, *Case Stud. Therm. Eng.*, **28** (2021), 101537. https://doi.org/10.1016/j.csite.2021.101537

32. B. Ali, C. S. K. Raju, L. Ali, S. Hussain, T. Kamran, G-Jitter impact on magnetohydrodynamic non-Newtonian fluid over an inclined surface: Finite element simulation, *Chinese J. Phys.*, **71** (2021), 479–491. https://doi.org/10.1016/j.cjph.2021.03.020

33. B. Ali, I. Siddique, A. Ahmadian, N. Senu, L. Ali, A. Haider, Significance of Lorentz and Coriolis forces on dynamics of water based silver tiny particles via finite element simulation, *Ain Shams Eng. J.*, **13** (2022), 101572. https://doi.org/10.1016/j.asej.2021.08.014

34. S. Kumar, K. Sharma, Mathematical modeling of MHD flow and radiative heat transfer past a moving porous rotating disk with Hall effect, *Multidiscip. Model. Ma.*, **18** (2022), 445–458. https://doi.org/10.1108/MMMS-04-2022-0056

AIMS Press